

Article

Lifetime Degradation Cost Analysis for Li-ion Batteries in the Capacity Market Using Accurate Physics-based Models

Ahmed Gailani*, Maher Al-Greer, Michael Short, Tracey Crosbie, and Nashwan Dawood

School of Computing, Engineering and Digital Technologies, Teesside University, Middlesbrough, TS1 3BX, UK; M.Al-Greer@tees.ac.uk (M.A.-G.); M.Short@tees.ac.uk (M.S.); T.Crosbie@tees.ac.uk (T.C.); N.N.Dawood@tees.ac.uk (N.D.)

* Correspondence: A.Gailani@tees.ac.uk; Tel.: +44-(0) 16-4221-8121

Received: date; Accepted: date; Published: date

Abstract: Energy storage devices provide services in the capacity market (CM). Li-ion batteries are a popular type of energy storage devices used in CM. Battery lifetime is a key factor in determining the economic viability of Li-ion batteries and current approaches to estimating this are limited. This paper explores the potential of a lithium-ion battery to provide CM services with four de-rating factors (0.5h, 1h, 2h and 4h). During the CM contract, the battery experiences both calendar and cycle degradation which reduces the overall profit. Physics-based battery and degradation models are used to quantify degradation cost for the battery in the CM to enhance earlier research results. The degradation model quantifies capacity losses related to solid-electrolyte interphase (SEI) layer, active material loss and SEI crack growth. Results show that the physics-based degradation model can accurately predict degradation cost at different operating conditions thus can substantiate the business case of the battery in the CM. The simulated CM profit can be higher by 60% and 75% at 5°C and 25° respectively compared to empirical and semi-empirical degradation models. A sensitivity analysis for a range of parameters are given to show their effects on batteries' overall profit.

Keywords: Capacity market, degradation cost, physics-based modelling, de-rating factors

1. Introduction

The threat of climate change due to global warming has encouraged many countries to adopt policies to increase reliance on renewable energy sources (RES) in their electricity networks. The EU policies require European countries to increase the energy produced by RES by 20% by 2020 and 27% by 2030 [1]. The total world renewable energy generation capacity increased by 14.5% in 2019 [2]. The intermittent nature of RES [3] along with fast energy demand growth [4] raises considerable energy security concerns [5,6]. Driven by such concerns, several multi-dimensional approaches have been used to ensure adequate and cost-efficient power systems. These include enabling innovative technologies such as energy storage [7-9], improving market design [10,11], and enhancing system operation [12].

The introduction of the capacity markets (CMs) to improve the electricity market design is seen as an effective solution to enabling the integration of RES in electricity networks. As such, CMs have been implemented in many countries including the US [13], Latin America [14], and Europe [15]. The aim of which, is to adequately remunerate new electrical generators, to reduce investment risks and avoid electricity blackouts. Many of the new generators participating in the CM are using Lithium-Ion batteries (LIBs) due to their high energy density and life cycle [16]. Earlier work has illustrated that batteries can enhance new generators business case by providing capacity services ranging from 40% to 100% of their nameplate capacity, thus reducing the number of shortage events (SE) in the

CM [17,18]. Other studies have found that the revenue from energy storage devices can be tripled if they are utilised to provide energy reserve services in the electricity markets [19]. Further work has found that batteries participating in the CM can secure substantial upfront revenue while only marginally reducing profits from other markets [20].

LIB degradation is the main factor in determining its operational cost [21]. As such, accounting for it is essential to assess the economic viability of LIBs in the CM. Once a battery wins a CM contract, it must remain ready to discharge during electricity SEs leaving the battery at 100% charge status for a long period, thus increasing its degradation cost [22]. The failure to deliver the contracted CM capacity when needed may result in penalties [23]. However, many previous studies that aim to evaluate the viability of LIBs in different grid applications either did not account for the degradation cost or there is no clear or accurate degradation model used. Earlier research in [24–26] studied how different batteries can provide ancillary services to the grid—such as short time operating reserve or capacity reserve—but this work did not include consideration of battery degradation. Other research in [20,27–29] evaluated the applicability of LIBs to provide different services such as spinning reserve, frequency response and peaking capacity, however once again these works did not include a clear battery degradation models. Many other studies accounted for degradation cost by including an empirical LIB degradation model [30–34]. These models are based on mathematical functions that provide good fitting for the experimental data used. While empirical and semi-empirical models are computationally efficient, they are usually based on limited battery operating conditions, thus making the extrapolation beyond the dataset used inaccurate [35,36].

Other empirical degradation models used often ignore important degradation details. For instance, earlier research in [37] presents a nonlinear degradation model to account for the degradation cost in the day ahead market while ignoring calendar degradation. However, in an actual island grid-connected battery operating for three years, it is found that the battery was in idling position for 20% of the total operating time [38] thus ignoring calendar may lead to erroneous results. Several other works either not considering temperature effects on battery degradation [39,40], overlooking State of Charge (SoC) effects during calendar degradation [41], or accounting for the impact of depth of discharge (DoD) only [42].

Other works consider the effects of degradation cost using advanced physics-based LIB models. The authors in [43] present a modelling framework for grid-connected batteries using physics-based single particle model (SPM) that consider capacity fade due to solid electrolyte interphase (SEI) layer mechanism. Similarly, the work in [44] presents a physics based SEI layer degradation assessment for LIBs in grid connected PV system using SPM. Recent research [45] uses different LIB models, including SPM, to optimise the battery to provide energy arbitrage service to the grid and concluded that the expected revenue could be substantially improved using more accurate battery degradation models. However, all the aforementioned works either do not consider the CM, or consider it without de-rating factors or quantifying one degradation mechanism (SEI layer only) for economic analysis while overlooking the impacts of other possible degradation effects such as active material loss and crack growth [46].

This paper improves on the previous economic studies by quantifying the degradation cost for three degradation mechanisms for LIB cells in the CM using physics-based degradation model coupled with a pseudo 2-dimensional LIB cell model. These three degradation mechanisms are SEI layer growth, active material (AM) loss and SEI layer fracture. Furthermore, this work considers several CM de-rating factors which is seen as essential in improving the business case for energy storage in the CM [47]. Ultimately, this work mitigates the limitation mentioned in a recent study [48] which concluded that empirical and semi-empirical degradation models are unable to capture battery degradation effects at lower temperatures such as 5°C.

2. Capacity Market Fundamentals

The reliability of liberalised electricity markets is questioned due to increasing energy demand, the decommissioning of conventional power plants (i.e. coal) and the steady growth of RES. In particular, many policymakers argue that the current energy-only markets may not ensure resource

adequacy [49]. One issue being that the energy-only market neglects the energy adequacy problem because it assumes that the energy demand and supply always balanced (quantity supplied=quantity demanded). Thus, when for instance, the supply side becomes scarce, there must be a load reduction from the demand side to ensure market clearance. However, due to the inelastic nature of the demand side and rational customer response, electricity markets do not guarantee a demand response or market clearance. [50].

Another reason for energy-only market failure is its inefficiency during electricity blackouts [51]. If there is a blackout similar to the one that happened in the UK in 2019 which affected over 1 million customers [52], then there is at least one supplier which does not have the power to sell at any price as illustrated in Figure 1a. Despite the scarce capacity and the peak demand, generators do not earn money in the blackout events[48].

Nevertheless, even if there are no generation adequacy issues, a 'missing money' problem exists in both normal operating conditions and scarcity periods. In normal operating conditions where the demand quantity is below the peak available capacity as shown in Figure 1b and the market is competitive, some generators such as the Peakers (plants operate only at high demand) cannot earn sufficient revenue beyond the operating cost [49]. Therefore, they may not cover their capital investment cost. In scarcity periods as shown in Figure 1c, all generators may earn high scarcity prices (red dot) which, in real cases, can be '367' times higher than the average price [53]. However, market power can be exercised in scarcity periods even by small generators (see [54]), therefore triggering regulatory intervention. Regulators usually set the scarcity prices low to mitigate market power abuse thus creating the missing money problem depicted in Figure 1c. Since the investment in new capacity to increase the reliability of the supply side depends on the scarcity prices, energy-only markets therefore do not provide the incentives needed to build new capacity.

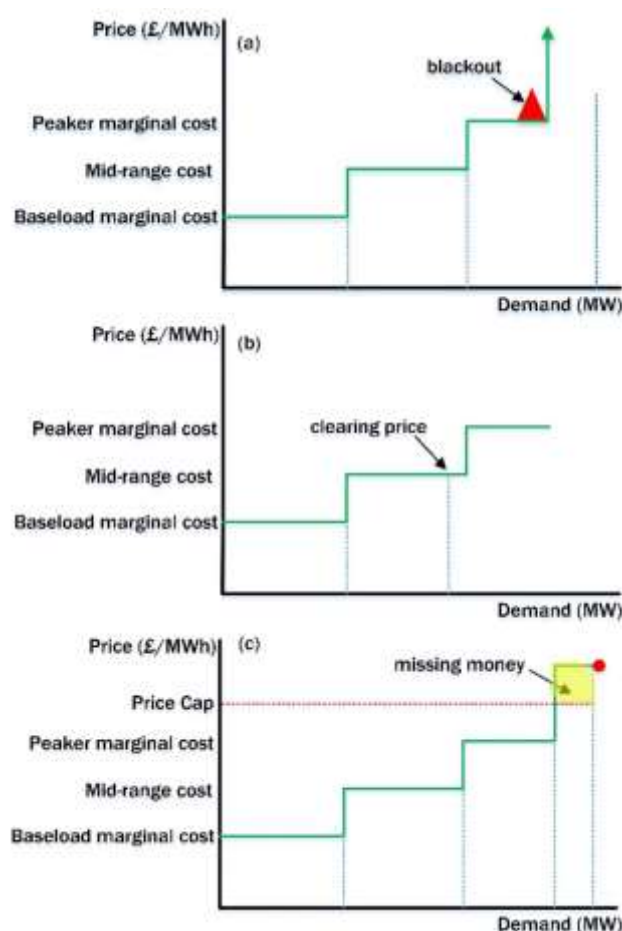


Figure 1. Energy price and demand for different generators during: (a) blackout; (b) normal operation; (c) period of scarcity

A well-designed CM can mitigate the issues of market power and missing money by determining the adequate level of supply capacity needed. This can be done by designing a capacity auction for generators to determine the scarcity price needed to secure the adequate level of capacity as set by the regulator to reduce the number of shortage hours. The auction is open to new and existing generators to consider the investment level needed in the new generators. The result is that the auction discovers the true value of the scarcity price corresponding to the optimal level of capacity while the regulatory intervention has been limited only to control the level of the capacity needed.

For several reasons, energy storage devices may have limited discharge capacity (for example, degradation). Therefore, CMs (in the UK, Germany, France, Italy, Ireland, and Denmark) have introduced de-rating methodologies to account for the percentage of firm capacity they can supply at shortage periods [55]. Fraunholz et al. [56] found that the choice of a suitable de-rating factor is challenging and may affect batteries' market competitiveness. Figure 2 shows the number of batteries participating in the current UK's CM with different de-rating factors. It can be seen that there is an increased interest in obtaining higher de-rating factors such as 3h or 4h. This study considers a real-life scenario in which the LIB is utilised to get 0.5h, 1h, 2h, and 4h de-rating factors.

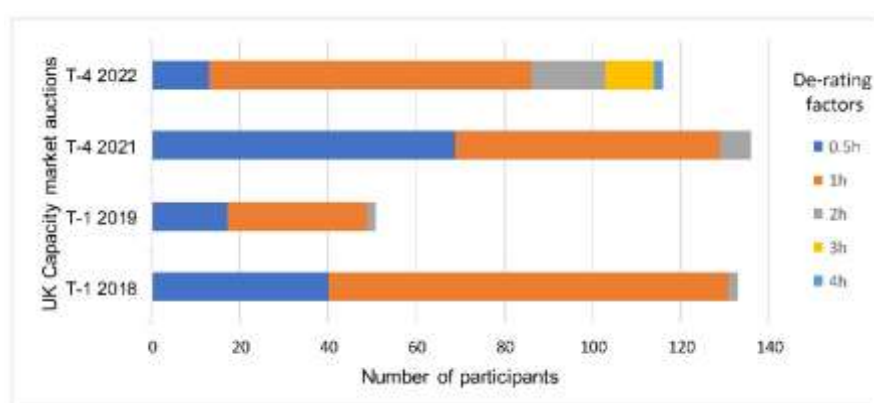


Figure 2. The number of batteries in the UK's capacity market from T-1 2018 to T-4 2022 for different de-rating factors.

3. Methods

3.1. Problem Setup

This study models battery degradation for LIB used to provide a CM service to the UK grid operator over a one year contract using a physics based model. During the contract's period, many simultaneous degradation mechanisms affect the battery performance which results in a degradation cost. As illustrated in Figure 3, when the CM's contract begins, the battery should provide reserve services to the grid and be ready to respond at electricity SEs. Therefore, in the absence of SEs, the calendar battery degradation can be quantified. During SEs and depending on its duration, the obligation capacity will be calculated for each de-rated battery. The duration of the event and the obligation capacity amount is updated at each settlement period (30 minutes). Then, a physics-based battery model is used to discharge the required capacity. The operating conditions of the battery such as the temperature are then fed to the degradation model to quantify cycle degradation and update the initial capacity in the model. Afterwards, depending on the amount of generated power, the penalties and overpayment can be quantified to obtain the overall revenue. The battery capacity and the de-rating factors used in this study are shown in Table.1 which are in line with the current batteries participating in the CM [57]. The CM parameters used in this study are given in earlier study [48].

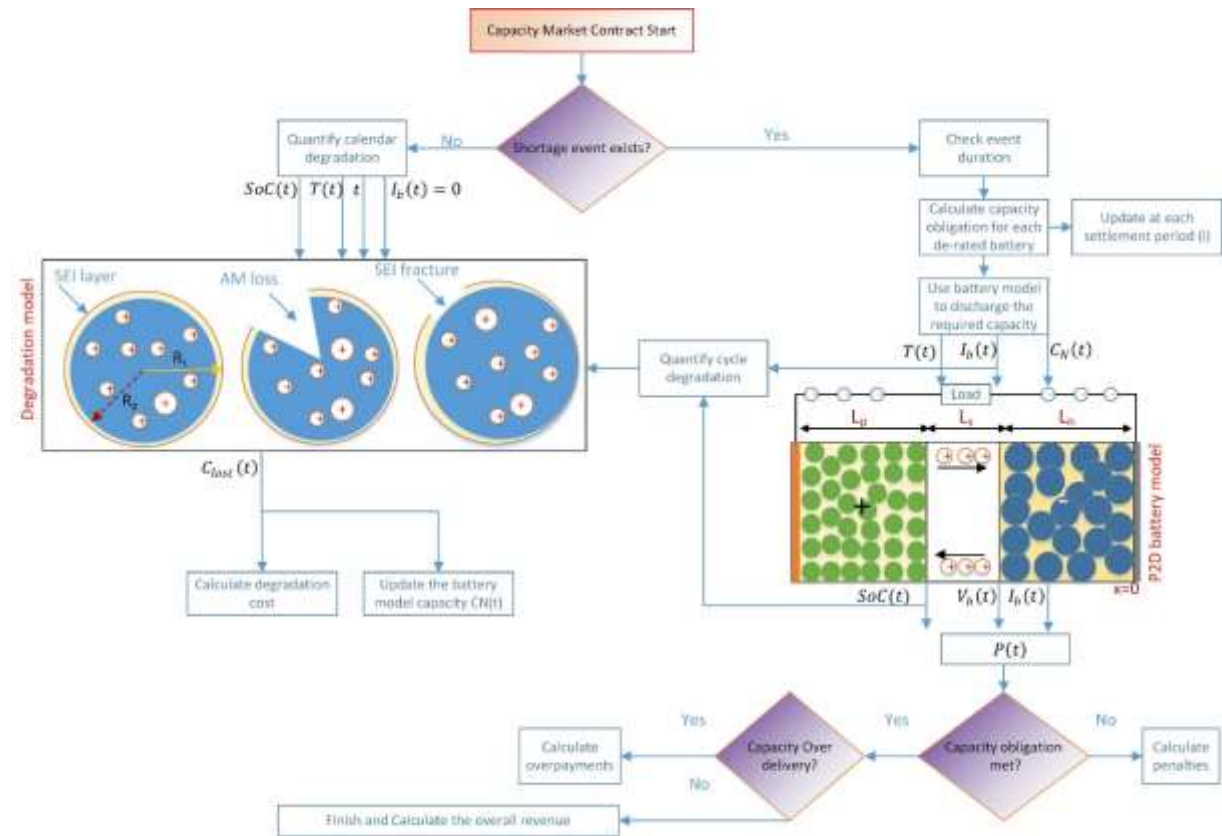


Figure 3. Revenue and degradation cost flow chart process in the capacity market

Table 1. The battery capacity and the de-rating factors used in this study

Battery Capacity (MWh)	Generated Power (MW)	De-rating (h)
2	2	0.5
2	2	1
2	1	2
2	0.5	4

The total revenue of the battery R represents the revenue from CM contract in addition to overpayments R_{ov} minus potential penalties p as given in (1) where C_{de} is the de-rated capacity, k_{de} is the de-rating factor, λ_{cl} is the CM auction clearing price, and f is a factor used to reward slightly more payment in peak demand months.

$$R = C_{de} \times \lambda_{cl} \times f + R_{ov} - p \quad (1)$$

The de-rated capacity C_{de} depends on the battery's output power as in (2) where $I_b(t)$ is the battery current, $V_b(t)$ is the battery voltage, and N is the total number of battery cells.

$$C_{de} = I_b(t) \times V_b(t) \times N \times k_{de} \quad (2)$$

The capacity obligation C_o is calculated at each settlement period (i) as in (3)-(4) where D_p is the peak electricity demand during the SE D_p^{se} divided by the total CM contracted capacity through the CM auction C_{auc} , and C_b is the capacity offered by the battery to other grid services.

$$C_o(i) = \sum_{i=1}^n (C_{de} \times D_p(i)) - C_b(i) \quad (3)$$

$$D_p(i) = \frac{D_{p(i)}^{se}}{C_{auc}} \quad (4)$$

The penalties and the overpayments are obtained by calculating the amount of undelivered/over delivered capacity over the CM contract at each settlement period as in (5)-(6)

$$p = \sum_{i=1}^t C_{un(i)} \times \lambda_{cl} \quad (5)$$

$$R_{ov} = \sum_{i=1}^t C_{ov(i)} \times \lambda_{cl} \quad (6)$$

By multiplying the lost battery capacity $C_{lost}(t)$ that is obtained from the battery degradation model by a degradation price λ_{degr} , the total energy degradation cost E_{lost} can be roughly estimated as in (7).

$$E_{lost} = C_{lost}(t) \times \lambda_{degr} \times N \quad (7)$$

3.2. Battery Cycling Profile

The battery cycles in the CM are calculated according to the SEs' period. The expected number of these SEs is based on the loss of load expectation (LOLE) reliability metric [58]. Since accurately predicting LOLE is difficult as it is a function of complex processes such as generator availability, blackouts, and environmental factors, thus many studies deem LOLE not reliable [59,60]. In the presence of high share of RESs, it is found that LOLE can reach 62 hour per year [61]. Another study found that LOLE can reach 83h per year considering the current CM scarcity prices [62]. Therefore, by considering the difficulty in estimating realistic LOLE and the previous studies, this work assumes that the total number of different duration SEs is 20 in the first year of the CM's contract while rising to 90 in another year (from month 13-24) as shown in Figure 4. This distribution of SEs considers the electricity peak demand periods in most parts of Europe [63]. Furthermore, the distribution reflects the probability of the duration of SEs, for instance, 1h and 2h are more probable than 4h events [64].

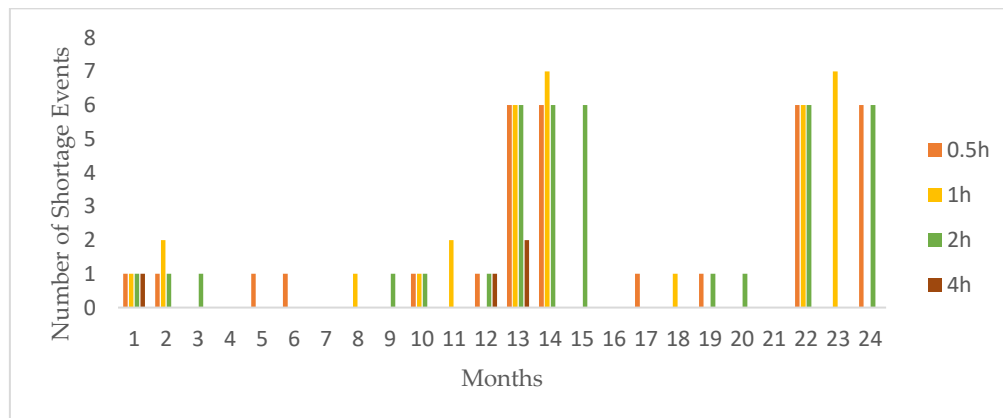


Figure 4. Battery cycling profile according to the number of expected shortage events in the capacity market

3.3. Battery and Degradation Models

3.3.1 Battery Model

The battery electrochemical cell model is shown in Figure 1 and based on the seminal work by Newman et al. [65]. The input to the model is the load current, material properties, geometry design parameters and the operating temperature. The output is the cell voltage and the SoC. The model parameters values used in this study are given in Appendix A. The five model states are; the lithium concentration in the solid (c_s) and electrolyte phase (c_e), the electric potential in the solid (ϕ_s) and electrolyte (ϕ_e) along with the rate of lithium movement between the phases (j^{Li}) [66]. These variables can be found by solving five coupled differential equations along with their boundary conditions as described below.

The mass conservation of lithium (assuming the concentration of lithium within the particles is spherically symmetric) in the solid phase can be described using Fick's second law in (8) where (D_s) is the solid phase diffusion constant and (r) is the radial (pseudo) dimension. The first boundary condition of (8) is given by (9) indicating that there is no diffusion in the centre of the particle. The second boundary condition is given by (10) indicating that the transfer of charges occur at the outer boundary of the particle where (a_s) is the specific interfacial area between the solid and the electrolyte, (R_p) is the particle radius and (F) is Faraday's constant.

$$\frac{\partial c_s}{\partial t} = \frac{D_s}{r^2} \frac{\partial}{\partial r} (r^2 \frac{\partial c_s}{\partial r}) \quad (8)$$

$$\left. \frac{\partial c_s}{\partial r} \right|_{r=0} = 0 \quad (9)$$

$$-D_s \left. \frac{\partial c_s}{\partial r} \right|_{r=R_p} = \frac{j^{Li}}{a_s F} \quad (10)$$

Lithium's concentration in the electrolyte phase is the result of diffusion (first term) and due to charge transfer between the solid and the electrolyte (second term) as in (11) where (ε_e) is the porosity and (t_0^+) is the transference number of the cation with respect to the solvent. Since there must be no electrolyte flux at the cell boundaries, the boundary conditions of (11) is given in (12).

$$\frac{\partial(\varepsilon_e c_e)}{\partial t} = \frac{\partial}{\partial x} \left(D_e^{eff} \frac{\partial c_e}{\partial x} \right) + \frac{1 - t_0^+}{F} j^{Li} \quad (11)$$

$$\left. \frac{\partial c_e}{\partial x} \right|_{x=L_n} = \left. \frac{\partial c_e}{\partial x} \right|_{x=L_p} = 0 \quad (12)$$

The solid phase charge conservation follows Ohm's law since (ϕ_s) depends on the current passing through the solid as in (13) where (σ^{eff}) is the effective conductivity. The current only flows at the collector/solid interface as in the boundary conditions in (14) where (A) is the electrode area.

$$\frac{\partial}{\partial x} (\sigma^{eff} \frac{\partial \phi_s}{\partial x}) = j^{Li} \quad (13)$$

$$-\sigma^{eff} \left. \frac{\partial \phi_s}{\partial x} \right|_{x=0} = -\sigma^{eff} \left. \frac{\partial \phi_s}{\partial x} \right|_{x=L_T} = \frac{I}{A} \quad (14)$$

$$-\sigma^{eff} \left. \frac{\partial \phi_s}{\partial x} \right|_{x=L_n} = -\sigma^{eff} \left. \frac{\partial \phi_s}{\partial x} \right|_{x=L_p} = 0$$

The electrolyte phase charge conservation follows Ohm's law in a liquid electrolyte (first term) and the local concentration of lithium (second term) as in (15) where (κ^{eff}) is the effective conductivity of the electrolyte. At the boundary of the electrode/current collector interphase, the ionic current must be zero as in (16) where:

$$\frac{\partial}{\partial x}(\kappa^{eff} \frac{\partial}{\partial x} \phi_e) + \frac{\partial}{\partial x}(\kappa_D^{eff} \frac{\partial}{\partial x} \ln c_e) = j^{Li} \quad (15)$$

$$\frac{\partial \phi_e}{\partial x} \Big|_{x=0} = \frac{\partial \phi_e}{\partial x} \Big|_{x=L_T} = 0 \quad (16)$$

The equations (8) -(16) are coupled through the Butler-Volmer equation in (17) where (i_o) is the exchange current density, (R) is the universal gas constant, (T) is the temperature, (α_a, α_c) are anode/cathode symmetry factor respectively, and (η) is the reaction overpotential.

$$j^{Li} = a_s i_o \left\{ \exp\left(\frac{\alpha_a F}{RT} \eta\right) - \exp\left(-\frac{\alpha_c F}{RT} \eta\right) \right\} \quad (17)$$

After solving the above equations, the cell voltage and SoC are given in (18) -(19):

$$V_b(t) = \phi_s(L_T, t) - \phi_s(0, t) \quad (18)$$

$$x = SoC \frac{c_{s,avg}^{pos}}{c_{s,max}^{pos}}, y = \frac{c_{s,avg}^{neg}}{c_{s,max}^{neg}} \quad (19)$$

3.3.2 Degradation Model

Several degradation mechanisms for LIBs are presented in the literature and various models are reported to describe these mechanisms with often more than one model to describe a single mechanism [36]. Here, three dominant aging mechanisms are included and shown in Figure 1: SEI layer growth, active material (AM) loss, and SEI layer fracture. For a complete derivation of these models please refer to [67-69]. The degradation model used in this work is dependent on the P2D battery model described in [70].

The total degradation equation that represents all the three mechanisms are given in (20). The SEI layer growth (Q_{SEI}) is directly proportional with the side reaction current density i_s and the governing equations related to it are given in (21)-(24). During charge/discharge process, the mechanical stress generated inside the active material could results in particle fracture which in turns may isolate the active material. As such, the lithium's amount is reduced leading to capacity loss (Q_{AM}) as given in (25). SEI fracture is observed in [71] where the SEI layer experiences tensile stress as the active material expands. This results in SEI layer stretch and cracking ($Q_{SEI,crack}$) which exacerbate the battery cell's harmful side reaction. The governing equations of ($Q_{SEI,crack}$) are given in (26)-(27). All the parameters used in this degradation model are given in Appendix B.

$$C_{lost}(t) = Q_{SEI} + Q_{AM} + Q_{SEI,crack} \quad (20)$$

$$Q_{SEI} = \int_0^t i_s(t) dt = \int_0^t \frac{k_{SEI} \exp\left(\frac{-E_{SEI}}{RT}\right)}{2(1 + \lambda\theta)\sqrt{t}} dt \quad (21)$$

$$\theta = \exp\left[\frac{F}{RT}(\eta_k + U_n^{OCP} - U_s^{OCP})\right] \quad (22)$$

$$\eta_k = \frac{2RT}{F} \ln\left(\xi + \sqrt{\xi^2 + 1}\right) \quad (23)$$

$$\xi = \frac{R_p I_b(t)}{6\varepsilon_{AM,0} i_o V} \quad (24)$$

$$Q_{AM} = \int_0^t SoC d\varepsilon_{AM} = \int_0^t k_{AM} \exp\left(\frac{-E_{AM}}{RT}\right) SoC |I_b(t)| dt \quad (25)$$

$$Q_{SEI,crack} = \sum_{k=1}^{N_c} Q_{SEI,crack} = k_{SEI,crack} \sum n_k(\sigma_k) \left(\frac{\sigma_k}{\sigma_{Yield}}\right)^{1/m} \quad (26)$$

$$\sigma_k = \frac{\sigma_{max,k} - \sigma_{min,k}}{2} \quad (27)$$

4. Results

4.1 Accuracy of Battery and Degradation Models

The output voltage against the battery capacity is shown in Figure 5a and 5b for different current rates and temperatures during discharge. The model results are in good agreement with the experimental data presented in [72] for the same 53Ah NMC cell. In Figure 5a, as expected, the higher the current rating, the lower is the battery capacity which is a common feature for many other LIB chemistries [73]. The battery capacity at 4C rate, for instance, is 49.7Ah in the first cycles meaning its coulombic efficiency is at 93.7% or lower compared to 56Ah at 0.25C rate.

Figure 5b shows the battery capacity and voltage for different temperatures at 1C rate plotted against their experimental data. It can be seen that at lower temperatures such as 5°C, the battery capacity predicted by the model is 48Ah compared to 47.5Ah obtained experimentally. This suggests that without any degradation, this LIB cell state of health is 89.6 % at 5°C because of the increased battery resistance at lower temperatures [74]. The model's average root mean square error is 1.1%.

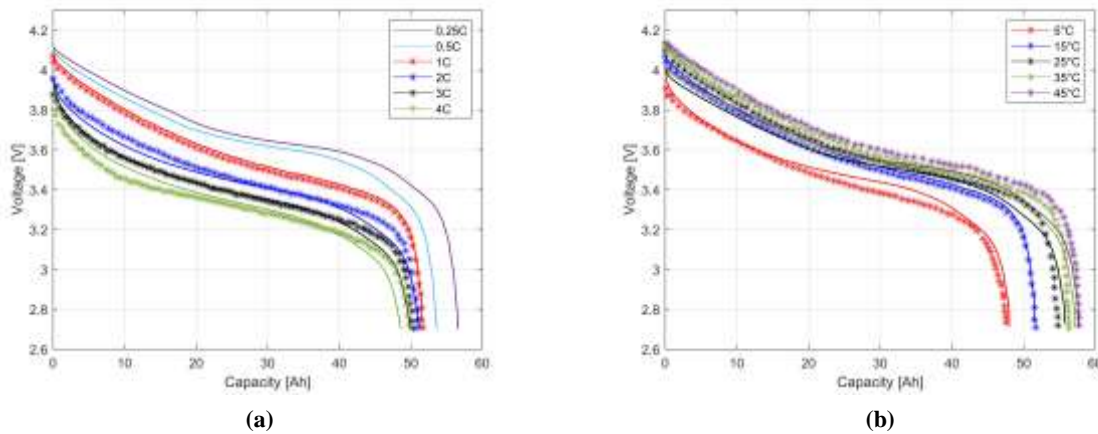


Figure 5. Battery model results (lines) with their experimental data (markers) during discharge based on [72] (a): for different C-rates and $T=15^{\circ}\text{C}$; (b) for different temperatures at 1C rate

The LIB cell degradation as predicted by equation (20) along with the corresponding experimental data are presented in Figure 6a for calendar degradation and Figure 6b for cycle degradation. The calendar experimental data are from [75] and the cycle experimental data are from [76]. The model results show good agreement with experiment data except for the results at temperature of 45°C at 100%SoC. In Figure 6a, high capacity loss is evident at higher temperatures and SoCs and vice-versa. For instance, at 5°C calendar, the LIB's state of health is over 96% after 500 days indicating that there is minimal capacity loss.

Figure 6b shows the cycling results for different C-rates at the same temperature 35°C except one at 5°C. The results indicated that the higher is the DoD, the higher the expected capacity loss at the same C-rate. Moreover, it can be seen that the cycling results at 5°C is as expected based on the battery model results obtained in Figure 5b in which the battery's state of health is 89% without any cycling then reaches 85% by the 2000 cycle. This mitigate the limitation of other models in which they are unable to capture that calendar degradation is minimum at lower temperatures while it can be maximum when cycling at the same lower temperatures [48]. This is important in applications where calendar and cycle degradation quantification are needed such as in the CM. In Figure 6c, a zoomed version of the 1C (100%DoD) is depicted to relate it to the three degradation mechanisms predicted by (21), (25) and (26). It can be seen that at higher DoD, the $Q_{SEI, crack}$ can be high in agreement with [70].

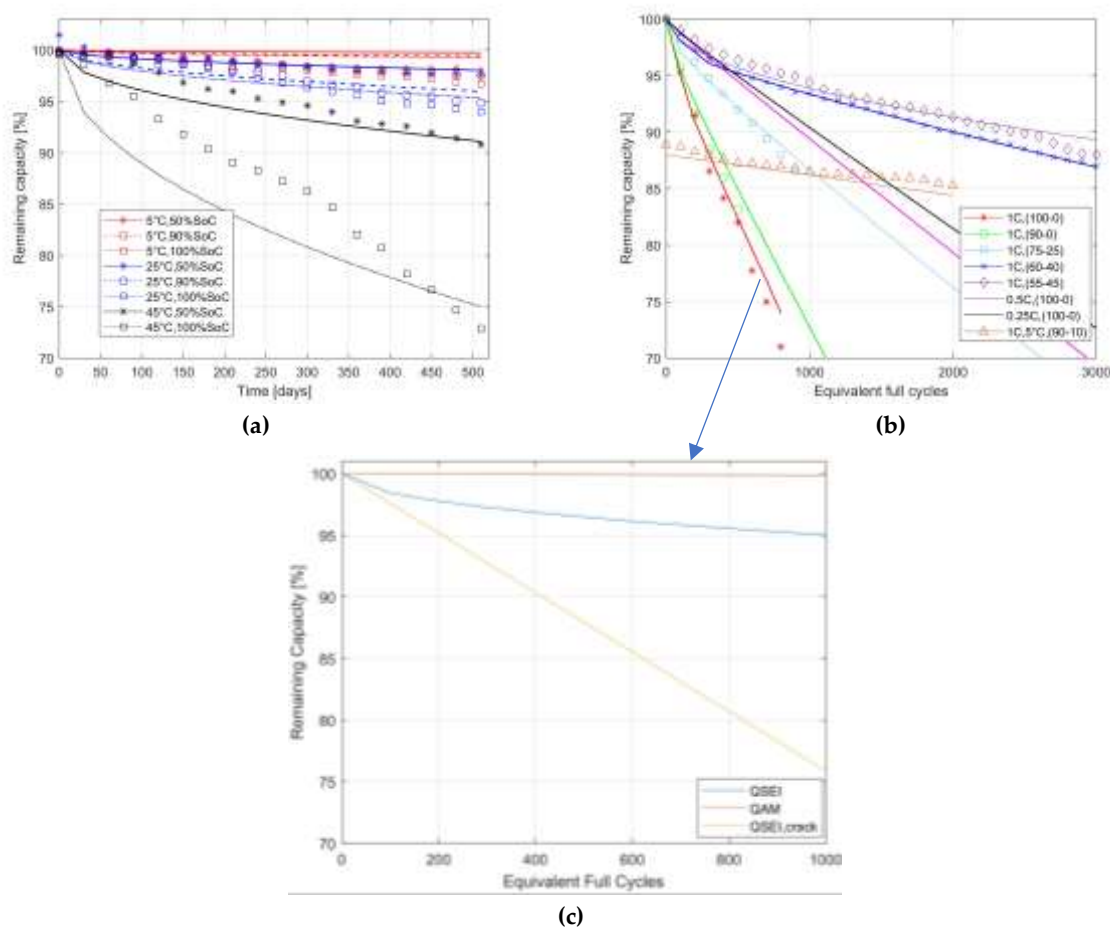


Figure 6. Battery degradation model results (lines) with their experimental data (markers) (a): calendar aging results with different temperatures and state of charges with experimental data from [75]; (b) cycle aging results with different depth of discharge ranges and C-rates at $T=35^{\circ}\text{C}$ with experimental data from [76] except the 1 data for 1C, 5°C (90-10) is from [75]; (c) detailed version for 1C(100-0) degradation based on the physics based degradation model mechanisms.

4.2. Revenue and degradation cost in the capacity market

The collected revenue over a 12 months CM contract along with any incurred degradation cost is depicted in Figure 7 and Figure 8 for the four de-rated batteries for different conditions. In Figure 7, the batteries were kept at a room temperature 25°C and the SoC is varied to account for a real case scenario whereby the battery can be at different SoC level in a thermally controlled environment until it is ready to respond to SEs. First, it can be seen that the 1h de-rated battery has the highest revenue compared to the others due to the relatively high k_{de} compared to its C_o . The modelling result is confirmed with a battery asset owners opting for a 1h de-rating factors in the most recent CM auction [77]. Second, the degradation cost is lower at low SoCs as the calendar degradation is generally low. Third, compared with the same cases presented in [48], the physics based degradation model predicts lower capacity losses at the same conditions hence offers the opportunity to get more overpayment represented by equation (6) as well as lowering the exposure to penalties (equation (5)) for the 4h de-rated battery. As such, the total collected revenues per CM contract is higher compared to the results presented in [48].

In Figure 8, the impact of the temperature change on the revenue is huge which necessities a battery thermal management system to keep the temperature controlled at lower temperatures. However, when discharge during SEs, it is necessary to lift the batter's temperature to respond effectively and avoid penalties. Since the cycling here is low during the first 12 months CM contract as shown in Figure 4, the average revenues stay the same with the 1h de-rated battery has the highest revenue.

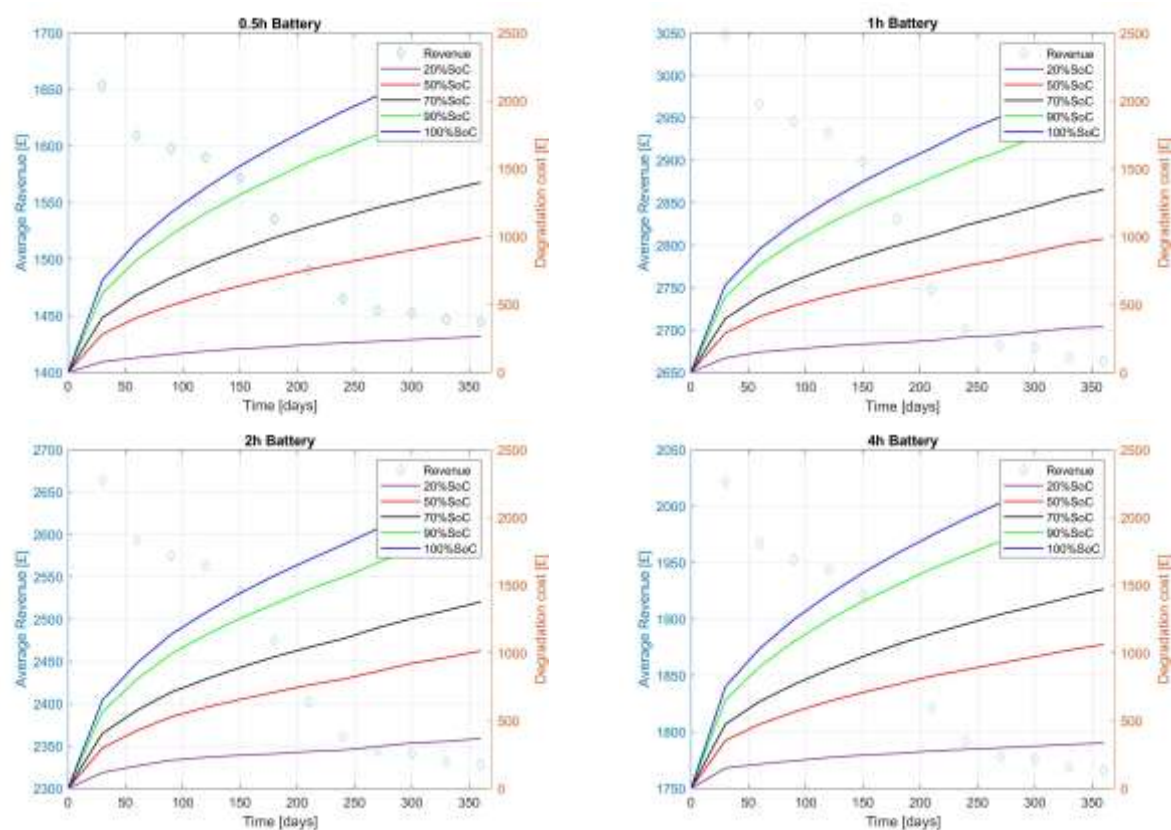


Figure 7. Revenue and degradation cost for four de-rated batteries (0.5h-4h) for one-year capacity market contract at different state of charges and $T=25^{\circ}\text{C}$.

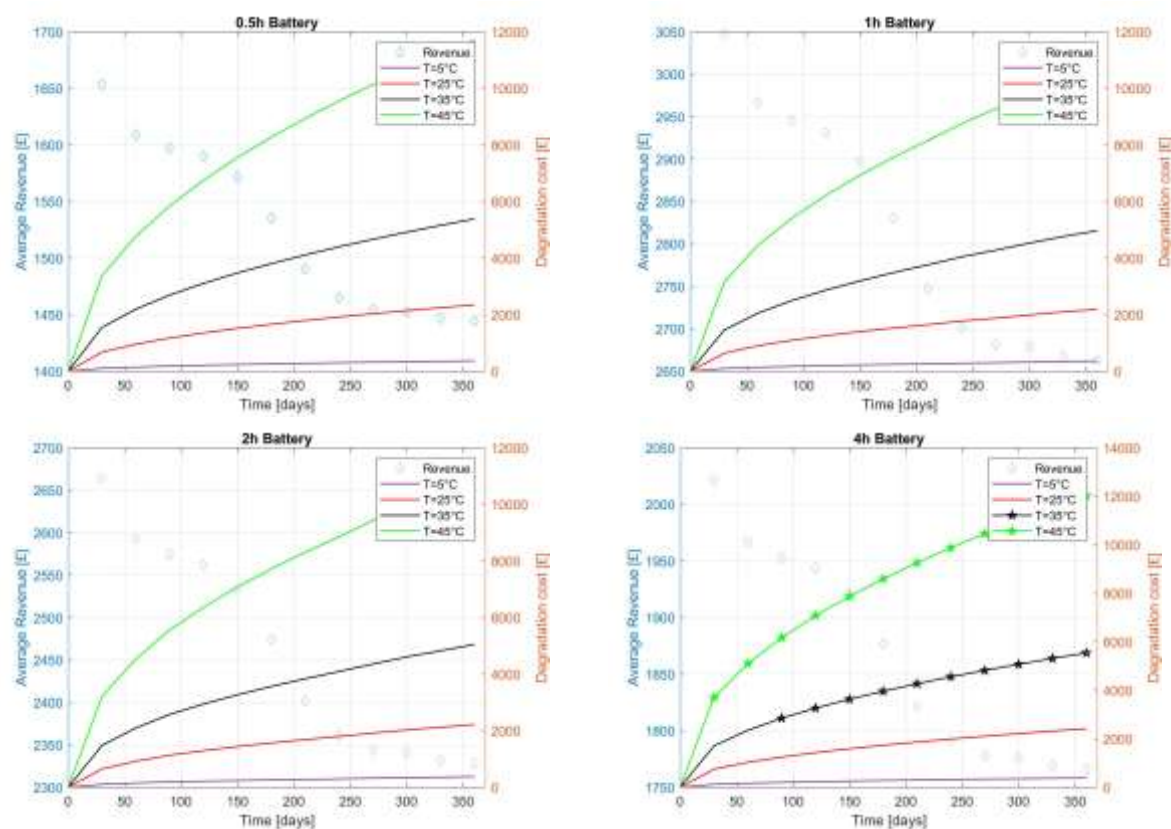


Figure 8. Revenue and degradation cost for four de-rated batteries (0.5h-4h) for one-year capacity market contract at different temperatures at 100% state of charge.

Table 2 summarises different degradation models accuracy which have been used in the same CM application to predict the degradation cost. These are an empirical and semi-empirical models reported in earlier study [48] and the physics based degradation model used in this study. The physics-based degradation model is more accurate than the other two to predict calendar and cycle degradation under different operating conditions. This is due to the feedback mechanism exists by using an accurate p2d battery cell model in which most of the parameters used account for temperature/C rate change as given in Appendix A. Also, although empirical and semi-empirical modes that are tied to equivalent circuit models can be useful and computationally fast, the process of dirtying the parameter values in these models uses empirical system identification. Therefore, changing the operating conditions necessitating a different fitting which is time-consuming and unreliable.

Table 2. Calendar and cycle degradation model accuracy comparison for different temperature

Temperatures	Degradation Model Type					
	Empirical		Semi-Empirical		Physics	
	calendar	cycle	calendar	cycle	calendar	cycle
Low temperatures (5°C onwards)	A	U	O	A	A	A
Medium temperatures (25°C onwards)	A	A	A	A	A	A
High temperatures (45°C onwards)	A	E	A	A	A	A

A:Accurate,U:underestimate degradation, O:overestimate degradation, E:Extrapolation by Arrhenius equation

In Table 3, the profit (revenue – degradation cost) for the 1h de-rated battery is calculated using the three different degradation model approaches (empirical, semi-empirical, and physics). By using a physics-based degradation model when accounting for the degradation cost, the profit can be higher by 59.6% and 75.5% for 5°C and 25°C if compared to both empirical and semi-empirical models. This is due to the lower degradation cost predicted which allows more overpayment to be collected. At higher temperatures such as 45°C, the physics model predicts higher losses compared to the other two.

Table 3. Profit at the end of 1-year capacity market contract for 1h de-rating factor battery when using several degradation models

Temperatures	Profit in (£) when degradation cost is calculated using below models		
	Empirical	Semi-Empirical	Physics
5°C	18862	-16962	31608
25°C	4716	12409	16417
45°C	-52580	-22054	-56284

4.3. Sensitivity Analysis

This section investigates the effects of changing important parameters on the profitability of the batteries participating in the CM. This include changes to CM clearance price, battery degradation cost, de-rating factors and increased SEs as a result of a predicted increase in energy demand. It should be noted that all the sensitivity analysis results are according to a standard temperature of 25°C except in 4.3.4 where the temperature was set to 5°C to study the effects of CM penalties.

4.3.1. Capacity Market Price Change Effects

CM clearing price λ_{cl} is an important parameter that can be changed with different CM auction results. As such, λ_{cl} has been changed twice to reflect the maximum and minimum auction price obtained in the UK's CM auctions from the start of the CM till now. The original $\lambda_{cl} = £19.4/\text{kW}/\text{year}$ has been changed to $\lambda_{cl} = £27.5/\text{kW}/\text{year}$ and $\lambda_{cl} = £6/\text{kW}/\text{year}$ [78,79]. Then, the profit (revenue – degradation cost) along one-year CM contract is depicted in Figure 9 and Figure 10 respectively for the four de-rated batteries. In Figure 9 and 10, it can be seen that λ_{cl} can hugely affect the batteries' profitability. In Figure 9, nearly all the four batteries are profitable at the end of the CM contract represented by an average increase of 167% compared to normal case. In Figure 10, all the four batteries incurred a huge loss due to low clearing price and high degradation cost represented by a decrease of 170% compared to normal case.

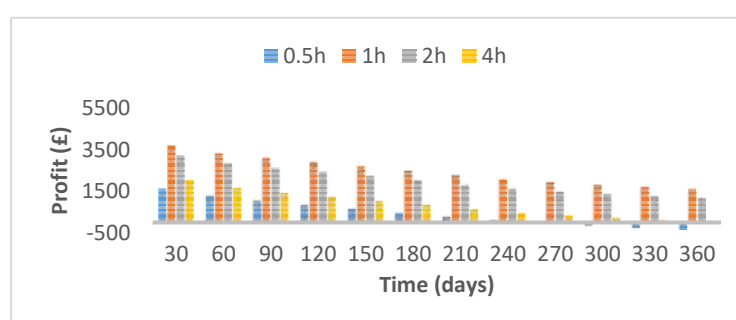


Figure 9. Profitability of the four de-rated batteries over 1-year when $\lambda_{cl} = £27.5/\text{kW}/\text{year}$

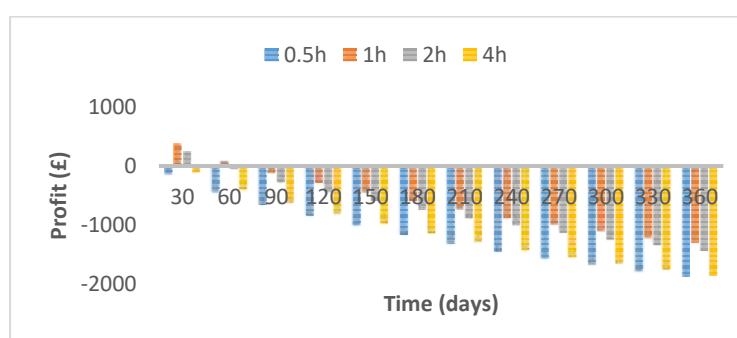


Figure 10. Profitability of the four de-rated batteries over 1-year when $\lambda_{cl} = £6/\text{kW}/\text{year}$

4.3.2. Degradation Cost Effects

The degradation cost is changed from 176\$/kWh or (0.5£/Ah) to an optimistic 100\$/kWh (0.29£/Ah) which is regarded as the ultimate goal for battery pack cost reduction in the future [80]. It can be seen in Figure 11 that all the batteries are profitable with an increase of nearly 50% in the standard case.

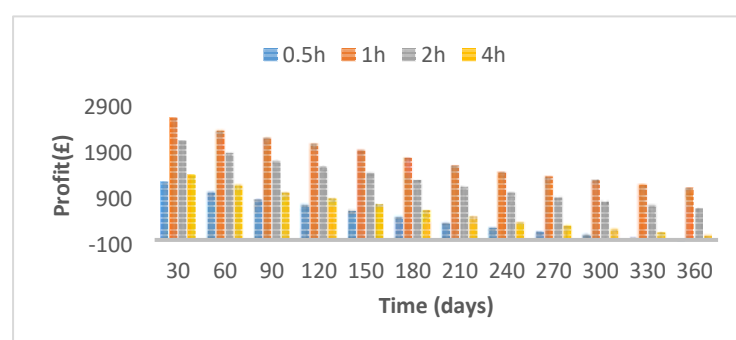


Figure 11. Profitability of the four de-rated batteries over 1-year when $\lambda_{degr} = \$100/\text{kWh}$

4.3.3. De-rating Factors Effects

The presumed de-rating factors for all the four batteries (0.5h to 4h) is projected to decrease in the future to allow for new generation entries in the CM as in [64]. Therefore, the de-rating factors have been changed accordingly to 17.80% for 0.5h battery, 36.44% for 1h battery, 64.79% for 2h battery and 96.11% for 4h battery. As shown in Figure 12, the overall profitability has been decreased with the 0.5h and 4h batteries are no longer profitable.

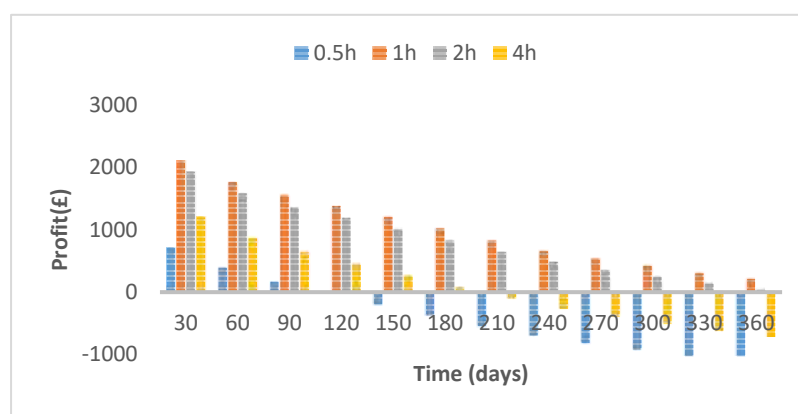


Figure 12. Profitability of the four de-rated batteries over 1-year when the de-rating factors changed

4.3.4. Increased Shortage Events in the CM

In case of expected increase in energy demand, the batteries in the CM are required to cycle more per year as shown in Figure 4 from month 13 to 24. In Figure 13, it can be seen that the 4h battery is totally unprofitable due to the incurred penalties when cycling because of the high amount of capacity obligation needed in which the battery cannot meet.

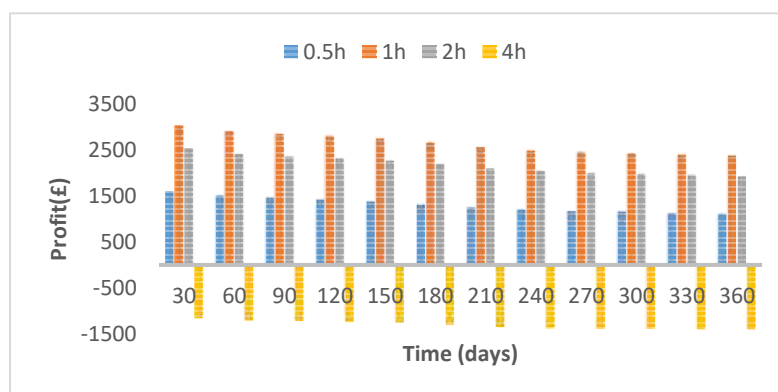


Figure 13. Profitability of the four de-rated batteries over 1-year when the shortage events increases

5. Conclusion and Future Work

This paper presented physics-based battery and degradation models that are used to inform degradation cost analysis for lithium-ion batteries in the CM. The degradation model considers the SEI layer growth, active material loss and SEI crack growth. The battery is utilised to obtain 0.5h, 1h, 2h and 4h CM de-rating factors. During a one-year CM contract, the battery experienced cycle and calendar degradation, which resulted in a degradation cost. At the same time, and depending on the batteries' capacity obligation, the de-rated batteries receive revenues, overpayment and penalties.

The results illustrate that the 1h de-rated battery can get the highest profit in the current CM design in all the simulated scenarios. The results also show that batteries providing CM services should be stored at low temperatures such as 5°C. However, during shortage periods when the

battery is delivering power, temperature should be lifted to 25°C to avoid penalties. Moreover, the physics-based degradation model accurately predicted calendar and cycle degradation for a wide range of temperature conditions compared to empirical and semi-empirical models. Due to lower predicted battery capacity loss, the batteries received more capacity overpayment thus increased the overall revenue. As such, the profit for the 1h de-rated battery was higher by 59.6% and 75.5% for 5°C and 25°C if compared to both empirical and semi-empirical models.

A sensitivity analysis for a range of parameters used in this study revealed that the CM profit can be affected in several ways. First, the profit for batteries is highly sensitive to CM auction price. For instance, increasing the CM auction price by 30% can increase the profit by nearly 170% for the 1h de-rated battery. Second, decreasing the degradation cost to optimal battery pack price of \$100/kWh can increase the profit by 50% for the 1h de-rated battery. Third, decreasing the de-rating reduced the profitability for the 0.5h and 4h de-rated batteries. Fourth, increased cycling in the case of high SEs hugely decreased the profitability of the 4h de-rated battery. Future work includes investigating how degradation can affect the overall CM design considering different regions and energy storage technologies.

Author Contributions: Conceptualization, A.G. and M.A.-G.; Methodology, A.G., M.A.-G.; Formal analysis, A.G., M.A.-G., M.S., N.D. and T.C.; Investigation, A.G., M.A.-G., M.S., N.D. and T.C.; Writing—Original draft preparation, A.G.; Writing—Review and editing, A.G., T.C., M.A.-G., N.D.; Supervision, T.C., N.D., M.A.-G. and M.S.

Funding: This research received no external funding.

Acknowledgments: Teesside University is gratefully acknowledged for fully supporting Ahmed's PhD study.

Conflicts of Interest: The authors declare no conflict of interest.

Appendix A: P2D battery model parameters

Parameters	Domain			Reference
	Positive electrode	Separator	Negative Electrode	
Bruggeman coefficient	1.5			
Faraday constant, F	96485			
Gas constant, R	8.314			
Thickness, L	41.16	17	74.83	[72]
Active material volume fraction, ε_s	0.43		0.55	[81]
Electrolyte volume fraction, ε_e	0.33	0.54	0.332	[81]
Particle size, r (μm)	11.3		27.2	a
Max. lithium concentration in the solid, $C_{s,max}$	88102		29934	a
Electrolyte initial lithium concentration		1200		[81]
Transference number, t_+^0	0.363	0.363	0.363	[66]
Activity dependence, f_{\pm}	1	1	1	[72]
Charge transfer coefficient, α_a, α_b	0.5		0.5	
Stoichiometry at 100% SoC, x_1, y_1	0.35		0.77	a
Stoichiometry at 0% SoC, x_0, y_0	0.92		0.02	a
Reference temperature, T_{ref}	298.15			
Electrical conductivity, σ	100		100	
Active material area, A	204mm		208mm	[72]

	*184mm	*188mm
Open circuit potential for positive electrode,	$-10.72x^4 + 23.88x^3 - 16.77x^2 + 2.595x + 4.563$ [82]	
Open circuit potential for negative electrode	$2.126y^4 - 5.511y^3 + 5.084y^2 - 2.036y + 0.4968$	
Electrolyte ionic conductivity, κ	$15.8C_e \times \exp(-13472C_e^{1.4}) \times \exp(\frac{-20000}{R}(\frac{1}{T} - \frac{1}{T_{ref}}))^2$ [72]	
Lithium diffusion in the electrolyte, D_e	$3.8037 \times 10^{-10} \times \exp(-0.792C_e) \times \exp(\frac{-10000}{R}(\frac{1}{T} - \frac{1}{T_{ref}}))$ [72]	
Lithium diffusion in the positive electrode $D_{s,pos}$	$3 \times 10^{-14} \times \exp(\frac{-35000}{R}(\frac{1}{T} - \frac{1}{T_{ref}}))^2$ [72]	
Lithium diffusion in the negative electrode $D_{s,neg}$	$3 \times 10^{-14} \times \exp(\frac{-35000}{R}(\frac{1}{T} - \frac{1}{T_{ref}}))^2$ [72]	
Reaction rate in the positive electrode, k_{pos}	$k_{0,pos}^{dis} \times \exp(-5x) \times \exp(\frac{-20000}{R}(\frac{1}{T} - \frac{1}{T_{ref}}))^2$	
	$k_{0,pos}^{ch} \times \exp(\frac{-20000}{R}(\frac{1}{T} - \frac{1}{T_{ref}}))^2$ [72]	
Reaction rate in the negative electrode, k_{neg}	$k_{0,neg}^{dis} \times \exp(\frac{-20000}{R}(\frac{1}{T} - \frac{1}{T_{ref}}))^2$ [72]	
	$k_{0,neg}^{ch} \times \exp(-5y) \times \exp(\frac{-20000}{R}(\frac{1}{T} - \frac{1}{T_{ref}}))^2$	

416 a:parameters estimation

417 Appendix B: Degradation model parameters

Parameter	Value
k_{SEI}	5.223×10^5
k_{AM}	7.88×10^{-3}
$k_{SEI,crack}$	2.22×10^{-7}
E_{SEI}	61276
E_{AM}	39600
λ	0.0148
V	1.2×10^{-5}
R_p	9×10^{-6} [68]
R_s	9.2×10^{-6} [68]
$\varepsilon_{AM,0}$	0.54
i_0	0.05
σ_{Yield}	8 [70]
m	0.5
$E_{Y,s}$	0.42
$E_{Y,p}$	14.3
v_s	0.2 [70]
v_p	0.3[70]

σ_k	$\frac{\sigma_{max,k} - \sigma_{min,k}}{2}$
$\sigma_{max,k}$	$\frac{E_{Y,s}}{(1-2vs)} b_1 + \frac{E_{Y,s}}{R_p^3(1+vs)} b_2$
$\sigma_{min,k}$	$\frac{E_{Y,s}}{(1-2vs)} b_1 + \frac{E_{Y,s}}{R_s^3(1+vs)} b_2$
b_1	$\frac{-2E_{Y,p}(2vs-1) \int_0^{R_p} \Omega_p(c_{LI}(r,t) - c_{LI}(r,0)) r^2 dr}{E_{Y,p}(2R_p^3 + R_s^3 - 4R_p^3vs + R_s^3vs) + E_{Y,s}(2R_s^3 - 2R_p^3 + 4R_p^3vp - 4R_s^3vs)} [70]$
b_2	$\frac{E_{Y,p}R_s^3(vs+1) \int_0^{R_p} \Omega_p(c_{LI}(r,t) - c_{LI}(r,0)) r^2 dr}{E_{Y,p}(2R_p^3 + R_s^3 - 4R_p^3vs + R_s^3vs) + E_{Y,s}(2R_s^3 - 2R_p^3 + 4R_p^3vp - 4R_s^3vs)} [70]$

418

419 **References**

- 420 1. Cucchiella, F.; D'Adamo, I.; Gastaldi, M. Future Trajectories of Renewable Energy Consumption in the
 421 European Union. *Resources* **2018**, *7*, doi:10.3390/resources7010010.
- 422 2. British Petroleum. *BP Statistical Review of World Energy*; London, UK, 2019; Available online:
 423 [https://www.bp.com/content/dam/bp/business-sites/en/global/corporate/pdfs/energy-](https://www.bp.com/content/dam/bp/business-sites/en/global/corporate/pdfs/energy-economics/statistical-review/bp-stats-review-2019-renewable-energy.pdf)
 424 [economics/statistical-review/bp-stats-review-2019-renewable-energy.pdf](https://www.bp.com/content/dam/bp/business-sites/en/global/corporate/pdfs/energy-economics/statistical-review/bp-stats-review-2019-renewable-energy.pdf) (accessed on 16/01/2020).
- 425 3. Kumar, J.; Parthasarathy, C.; Västi, M.; Laaksonen, H.; Shafie-Khah, M.; Kauhaniemi, K. Sizing and
 426 Allocation of Battery Energy Storage Systems in Åland Islands for Large-Scale Integration of
 427 Renewables and Electric Ferry Charging Stations. *Energies* **2020**, *13*, doi:10.3390/en13020317.
- 428 4. Khalili, S.; Rantanen, E.; Bogdanov, D.; Breyer, C. Global Transportation Demand Development with
 429 Impacts on the Energy Demand and Greenhouse Gas Emissions in a Climate-Constrained World.
 430 *Energies* **2019**, *12*, doi:10.3390/en12203870.
- 431 5. Lisin, E.; Strielkowski, W.; Chernova, V.; Fomina, A. Assessment of the Territorial Energy Security in
 432 the Context of Energy Systems Integration. *Energies* **2018**, *11*, doi:10.3390/en11123284.
- 433 6. Heylen, E.; Deconinck, G.; Van Hertem, D. Review and classification of reliability indicators for power
 434 systems with a high share of renewable energy sources. *Renewable and Sustainable Energy Reviews* **2018**,
 435 *97*, 554-568, doi:<https://doi.org/10.1016/j.rser.2018.08.032>.
- 436 7. Short, M.; Crosbie, T.; Dawood, M.; Dawood, N. Load forecasting and dispatch optimisation for
 437 decentralised co-generation plant with dual energy storage. *Applied Energy* **2017**, *186*, 304-320,
 438 doi:<https://doi.org/10.1016/j.apenergy.2016.04.052>.
- 439 8. Park, S.-H.; Hussain, A.; Kim, H.-M. Impact Analysis of Survivability-Oriented Demand Response on
 440 Islanded Operation of Networked Microgrids with High Penetration of Renewables. *Energies* **2019**, *12*,
 441 doi:10.3390/en12030452.
- 442 9. Kong, Q.; Fowler, M.; Entchev, E.; Ribberink, H.; McCallum, R. The Role of Charging Infrastructure in
 443 Electric Vehicle Implementation within Smart Grids. *Energies* **2018**, *11*, doi:10.3390/en11123362.
- 444 10. Strielkowski, W.; Streimikiene, D.; Fomina, A.; Semenova, E. Internet of Energy (IoE) and High-
 445 Renewables Electricity System Market Design. *Energies* **2019**, *12*, doi:10.3390/en12244790.
- 446 11. Tucki, K.; Orynycz, O.; Wasiak, A.; Świć, A.; Dybaś, W. Capacity Market Implementation in Poland:
 447 Analysis of a Survey on Consequences for the Electricity Market and for Energy Management. *Energies*
 448 **2019**, *12*, doi:10.3390/en12050839.

12. Gerard, H.; Rivero Puente, E.I.; Six, D. Coordination between transmission and distribution system operators in the electricity sector: A conceptual framework. *Utilities Policy* **2018**, *50*, 40–48, doi:<https://doi.org/10.1016/j.jup.2017.09.011>.
13. Albertus, P.; Manser, J.S.; Litzelman, S. Long-Duration Electricity Storage Applications, Economics, and Technologies. *Joule* **2020**, *4*, 21–32, doi:<https://doi.org/10.1016/j.joule.2019.11.009>.
14. Mastropietro, P.; Rodilla, P.; Batlle, C. De-rating of wind and solar resources in capacity mechanisms: A review of international experiences. *Renewable and Sustainable Energy Reviews* **2019**, *112*, 253–262, doi:<https://doi.org/10.1016/j.rser.2019.05.053>.
15. Bublitz, A.; Keles, D.; Zimmermann, F.; Fraunholz, C.; Fichtner, W. A survey on electricity market design: Insights from theory and real-world implementations of capacity remuneration mechanisms. *Energy Economics* **2019**, *80*, 1059–1078, doi:<https://doi.org/10.1016/j.eneco.2019.01.030>.
16. Lee, A.; Vörös, M.; Dose, W.M.; Niklas, J.; Poluektov, O.; Schaller, R.D.; Iddir, H.; Maroni, V.A.; Lee, E.; Ingram, B., et al. Photo-accelerated fast charging of lithium-ion batteries. *Nature Communications* **2019**, *10*, 4946, doi:10.1038/s41467-019-12863-6.
17. Sioshansi, R.; Madaeni, S.H.; Denholm, P. A Dynamic Programming Approach to Estimate the Capacity Value of Energy Storage. *IEEE Transactions on Power Systems* **2014**, *29*, 395–403, doi:10.1109/TPWRS.2013.2279839.
18. Khan, A.S.M.; Verzijlbergh, R.A.; Sakinci, O.C.; De Vries, L.J. How do demand response and electrical energy storage affect (the need for) a capacity market? *Applied Energy* **2018**, *214*, 39–62, doi:<https://doi.org/10.1016/j.apenergy.2018.01.057>.
19. Staffell, I.; Rustomji, M. Maximising the value of electricity storage. *Journal of Energy Storage* **2016**, *8*, 212–225, doi:<https://doi.org/10.1016/j.est.2016.08.010>.
20. Teng, F.; Strbac, G. Business cases for energy storage with multiple service provision. *Journal of Modern Power Systems and Clean Energy* **2016**, *4*, 615–625, doi:10.1007/s40565-016-0244-1.
21. Xu, B.; Oudalov, A.; Ulbig, A.; Andersson, G.; Kirschen, D.S. Modeling of Lithium-Ion Battery Degradation for Cell Life Assessment. *IEEE Transactions on Smart Grid* **2018**, *9*, 1131–1140, doi:10.1109/TSG.2016.2578950.
22. Castagneto Gisse, G.; Dodds, P.E.; Radcliffe, J. Market and regulatory barriers to electrical energy storage innovation. *Renewable and Sustainable Energy Reviews* **2018**, *82*, 781–790, doi:<https://doi.org/10.1016/j.rser.2017.09.079>.
23. Chen, H.; Baker, S.; Benner, S.; Berner, A.; Liu, J. PJM Integrates Energy Storage: Their Technologies and Wholesale Products. *IEEE Power and Energy Magazine* **2017**, *15*, 59–67, doi:10.1109/MPE.2017.2708861.
24. Kumar, A.; Meena, N.K.; Singh, A.R.; Deng, Y.; He, X.; Bansal, R.C.; Kumar, P. Strategic integration of battery energy storage systems with the provision of distributed ancillary services in active distribution systems. *Applied Energy* **2019**, *253*, 113503, doi:<https://doi.org/10.1016/j.apenergy.2019.113503>.
25. Askeland, M.; Jaehnert, S.; Korpås, M. Equilibrium assessment of storage technologies in a power market with capacity remuneration. *Sustainable Energy Technologies and Assessments* **2019**, *31*, 228–235, doi:<https://doi.org/10.1016/j.seta.2018.12.012>.
26. Haas, J.; Cebulla, F.; Nowak, W.; Rahmann, C.; Palma-Behnke, R. A multi-service approach for planning the optimal mix of energy storage technologies in a fully-renewable power supply. *Energy Conversion and Management* **2018**, *178*, 355–368, doi:<https://doi.org/10.1016/j.enconman.2018.09.087>.

27. Lorenzi, G.; da Silva Vieira, R.; Santos Silva, C.A.; Martin, A. Techno-economic analysis of utility-scale energy storage in island settings. *Journal of Energy Storage* **2019**, *21*, 691-705, doi:<https://doi.org/10.1016/j.est.2018.12.026>.
28. Greenwood, D.M.; Lim, K.Y.; Patsios, C.; Lyons, P.F.; Lim, Y.S.; Taylor, P.C. Frequency response services designed for energy storage. *Applied Energy* **2017**, *203*, 115-127, doi:<https://doi.org/10.1016/j.apenergy.2017.06.046>.
29. Denholm, P.; Nunemaker, J.; Gagnon, P.; Cole, W. The potential for battery energy storage to provide peaking capacity in the United States. *Renewable Energy* **2019**, *1*, doi:1.
30. Andrenacci, N.; Chiodo, E.; Lauria, D.; Mottola, F. Life Cycle Estimation of Battery Energy Storage Systems for Primary Frequency Regulation. *Energies* **2018**, *11*, doi:10.3390/en1123320.
31. Martins, R.; Hesse, C.H.; Jungbauer, J.; Vorbuchner, T.; Musilek, P. Optimal Component Sizing for Peak Shaving in Battery Energy Storage System for Industrial Applications. *Energies* **2018**, *11*, doi:10.3390/en11082048.
32. Xu, B.; Zhao, J.; Zheng, T.; Litvinov, E.; Kirschen, D.S. Factoring the Cycle Aging Cost of Batteries Participating in Electricity Markets. *IEEE Transactions on Power Systems* **2018**, *33*, 2248-2259, doi:10.1109/TPWRS.2017.2733339.
33. Kies, A. Joint optimisation of arbitrage profits and battery life degradation for grid storage application of battery electric vehicles. *Journal of Physics: Conference Series* **2018**, *977*, 012005, doi:10.1088/1742-6596/977/1/012005.
34. Petit, M.; Prada, E.; Sauvart-Moynot, V. Development of an empirical aging model for Li-ion batteries and application to assess the impact of Vehicle-to-Grid strategies on battery lifetime. *Applied Energy* **2016**, *172*, 398-407, doi:<https://doi.org/10.1016/j.apenergy.2016.03.119>.
35. Thompson, A.W. Economic implications of lithium ion battery degradation for Vehicle-to-Grid (V2X) services. *Journal of Power Sources* **2018**, *396*, 691-709, doi:<https://doi.org/10.1016/j.jpowsour.2018.06.053>.
36. Reniers, J.M.; Mulder, G.; Howey, D.A. Review and Performance Comparison of Mechanical-Chemical Degradation Models for Lithium-Ion Batteries. *Journal of The Electrochemical Society* **2019**, *166*, A3189-A3200, doi:10.1149/2.0281914jes.
37. Maheshwari, A.; Paterakis, N.G.; Santarelli, M.; Gibescu, M. Optimizing the operation of energy storage using a non-linear lithium-ion battery degradation model. *Applied Energy* **2020**, *261*, 114360, doi:<https://doi.org/10.1016/j.apenergy.2019.114360>.
38. Dubarry, M.; Devie, A.; Stein, K.; Tun, M.; Matsuura, M.; Rocheleau, R. Battery Energy Storage System battery durability and reliability under electric utility grid operations: Analysis of 3 years of real usage. *Journal of Power Sources* **2017**, *338*, 65-73, doi:<https://doi.org/10.1016/j.jpowsour.2016.11.034>.
39. Wankmüller, F.; Thimmapuram, P.R.; Gallagher, K.G.; Botterud, A. Impact of battery degradation on energy arbitrage revenue of grid-level energy storage. *Journal of Energy Storage* **2017**, *10*, 56-66, doi:<https://doi.org/10.1016/j.est.2016.12.004>.
40. Purvins, A.; Sumner, M. Optimal management of stationary lithium-ion battery system in electricity distribution grids. *Journal of Power Sources* **2013**, *242*, 742-755, doi:<https://doi.org/10.1016/j.jpowsour.2013.05.097>.
41. Pimm, A.J.; Palczewski, J.; Morris, R.; Cockerill, T.T.; Taylor, P.G. Community energy storage: A case study in the UK using a linear programming method. *Energy Conversion and Management* **2020**, *205*, 112388, doi:<https://doi.org/10.1016/j.enconman.2019.112388>.

42. Dufo-López, R.; Bernal-Aguistin, J.L. Techno-economic analysis of grid-connected battery storage. *Energy Conversion and Management* **2015**, *91*, 394–404, doi:<https://doi.org/10.1016/j.enconman.2014.12.038>.
43. Patsios, C.; Wu, B.; Chatzinikolaou, E.; Rogers, D.J.; Wade, N.; Brandon, N.P.; Taylor, P. An integrated approach for the analysis and control of grid connected energy storage systems. *Journal of Energy Storage* **2016**, *5*, 48–61, doi:<https://doi.org/10.1016/j.est.2015.11.011>.
44. Weißhar, B.; Bessler, W.G. Model-based degradation assessment of lithium-ion batteries in a smart microgrid. In Proceedings of 2015 International Conference on Smart Grid and Clean Energy Technologies (ICSGCE), 20–23 Oct. 2015; pp. 134–138.
45. Reniers, J.M.; Mulder, G.; Ober-Blöbaum, S.; Howey, D.A. Improving optimal control of grid-connected lithium-ion batteries through more accurate battery and degradation modelling. *Journal of Power Sources* **2018**, *379*, 91–102, doi:<https://doi.org/10.1016/j.jpowsour.2018.01.004>.
46. Birkel, C.R.; Roberts, M.R.; McTurk, E.; Bruce, P.G.; Howey, D.A. Degradation diagnostics for lithium ion cells. *Journal of Power Sources* **2017**, *341*, 373–386, doi:<https://doi.org/10.1016/j.jpowsour.2016.12.011>.
47. Usera, I.; Rodilla, P.; Burger, S.; Herrero, I.; Batlle, C. The Regulatory Debate About Energy Storage Systems: State of the Art and Open Issues. *IEEE Power and Energy Magazine* **2017**, *15*, 42–50, doi:10.1109/MPE.2017.2708859.
48. Gailani, A.; Al-Greer, M.; Short, M.; Crosbie, T. Degradation Cost Analysis of Li-Ion Batteries in the Capacity Market with Different Degradation Models. *Electronics* **2020**, *9*, doi:10.3390/electronics9010090.
49. Cramton, P.; Ockenfels, A. Economics and design of capacity markets for the power sector. In *Interdisziplinäre Aspekte der Energiewirtschaft*, Springer: 2016; pp. 191–212.
50. Cramton, P.; Ockenfels, A.; Stoft, S. Capacity Market Fundamentals. *Economics of Energy & Environmental Policy* **2013**, Volume 2.
51. Ashokkumar Parmar, A.; Pranav B Darji, B. Capacity market functioning with renewable capacity integration and global practices. *The Electricity Journal* **2020**, *33*, 106708, doi:<https://doi.org/10.1016/j.tej.2019.106708>.
52. Energy Emergencies Executive Committee (E3C). *GB power system disruption on 9 August 2019*; UK, 2020; Available online: https://assets.publishing.service.gov.uk/government/uploads/system/uploads/attachment_data/file/855767/e3c-gb-power-disruption-9-august-2019-final-report.pdf (accessed on 03/02/2020).
53. Cramton, P. Electricity market design. *Oxford Review of Economic Policy* **2017**, *33*, 589–612, doi:10.1093/oxrep/grx041.
54. Sioshansi, F.P. *Competitive electricity markets: design, implementation, performance*; Elsevier: 2011.
55. Gailani, A.; Crosbie, T.; Al-Greer, M.; Short, M.; Dawood, N. On the Role of Regulatory Policy on the Business Case for Energy Storage in Both EU and UK Energy Systems: Barriers and Enablers. *Energies* **2020**, *13*, doi:10.3390/en13051080.
56. Fraunholz, C.; Keles, D.; Fichtner, W. *On the Role of Electricity Storage in Capacity Remuneration Mechanisms*; 2019.
57. National Grid. *Capacity Market Registers*; London, UK, 2019; Available online: <https://www.emrdeliverybody.com/CM/Registers.aspx> (accessed on 25 Apr 2019).
58. Slipac, G.; Zeljko, M.; Šljivac, D. Importance of Reliability Criterion in Power System Expansion Planning. *Energies* **2019**, *12*, doi:10.3390/en12091714.

59. Söder, L.; Tómasson, E.; Estanqueiro, A.; Flynn, D.; Hodge, B.-M.; Kiviluoma, J.; Korpås, M.; Neau, E.; Couto, A.; Pudjianto, D., et al. Review of wind generation within adequacy calculations and capacity markets for different power systems. *Renewable and Sustainable Energy Reviews* **2020**, *119*, 109540, doi:<https://doi.org/10.1016/j.rser.2019.109540>.
60. THEMA Consulting Group. *Capacity Adequacy in the Nordic Electricity Market*; Oslo, Norway, 2015; Available online: https://www.nordicenergy.org/wp-content/uploads/2015/08/capacity_adequacy_THEMA_2015-1.pdf (accessed on 16/03/2020).
61. Bhagwat, P.C.; Iychettira, K.K.; Richstein, J.C.; Chappin, E.J.L.; De Vries, L.J. The effectiveness of capacity markets in the presence of a high portfolio share of renewable energy sources. *Utilities Policy* **2017**, *48*, 76–91, doi:<https://doi.org/10.1016/j.jup.2017.09.003>.
62. Bhagwat, P.C.; Marcheselli, A.; Richstein, J.C.; Chappin, E.J.L.; De Vries, L.J. An analysis of a forward capacity market with long-term contracts. *Energy Policy* **2017**, *111*, 255–267, doi:<https://doi.org/10.1016/j.enpol.2017.09.037>.
63. Gallo Cassarino, T.; Sharp, E.; Barrett, M. The impact of social and weather drivers on the historical electricity demand in Europe. *Applied Energy* **2018**, *229*, 176–185, doi:<https://doi.org/10.1016/j.apenergy.2018.07.108>.
64. National Grid. *Duration-Limited Storage De-Rating Factor Assessment – Final Report*; London, UK, 2017; Available online: <https://www.emrdeliverybody.com/Lists/Latest%20News/Attachments/150/Duration%20Limited%20Storage%20De-Rating%20Factor%20Assessment%20-%20Final.pdf> (accessed on 18 Apr 2019).
65. Doyle, M. Modeling of Galvanostatic Charge and Discharge of the Lithium/Polymer/Insertion Cell. *Journal of The Electrochemical Society* **1993**, *140*, 1526, doi:10.1149/1.2221597.
66. Plett, G.L. *Battery Management Systems, Volume I: Battery Modeling*; Artech House: 2015.
67. Jin, X.; Vora, A.; Hoshing, V.; Saha, T.; Shaver, G.; García, R.E.; Wasynczuk, O.; Varigonda, S. Physically-based reduced-order capacity loss model for graphite anodes in Li-ion battery cells. *Journal of Power Sources* **2017**, *342*, 750–761, doi:<https://doi.org/10.1016/j.jpowsour.2016.12.099>.
68. Laresgoiti, I.; Käbitz, S.; Ecker, M.; Sauer, D.U. Modeling mechanical degradation in lithium ion batteries during cycling: Solid electrolyte interphase fracture. *Journal of Power Sources* **2015**, *300*, 112–122, doi:<https://doi.org/10.1016/j.jpowsour.2015.09.033>.
69. Prada, E.; Di Domenico, D.; Creff, Y.; Bernard, J.; Sauvant-Moynot, V.; Huet, F. A Simplified Electrochemical and Thermal Aging Model of LiFePO₄-Graphite Li-ion Batteries: Power and Capacity Fade Simulations. *Journal of The Electrochemical Society* **2013**, *160*, A616–A628, doi:10.1149/2.053304jes.
70. Jin, X.; Liu, C. Physics-based control-oriented reduced-order degradation model for LiNiMnCoO₂ - graphite cell. *Electrochimica Acta* **2019**, *312*, 188–201, doi:<https://doi.org/10.1016/j.electacta.2019.04.109>.
71. Zhang, H.-L.; Li, F.; Liu, C.; Tan, J.; Cheng, H.-M. New Insight into the Solid Electrolyte Interphase with Use of a Focused Ion Beam. *The Journal of Physical Chemistry B* **2005**, *109*, 22205–22211, doi:10.1021/jp053311a.
72. Hosseinzadeh, E.; Genieser, R.; Worwood, D.; Barai, A.; Marco, J.; Jennings, P. A systematic approach for electrochemical-thermal modelling of a large format lithium-ion battery for electric vehicle application. *Journal of Power Sources* **2018**, *382*, 77–94, doi:<https://doi.org/10.1016/j.jpowsour.2018.02.027>.
73. Li, J.; Wang, D.; Pecht, M. An electrochemical model for high C-rate conditions in lithium-ion batteries. *Journal of Power Sources* **2019**, *436*, 226885, doi:<https://doi.org/10.1016/j.jpowsour.2019.226885>.

74. Ouyang, D.; He, Y.; Weng, J.; Liu, J.; Chen, M.; Wang, J. Influence of low temperature conditions on lithium-ion batteries and the application of an insulation material. *RSC Advances* **2019**, *9*, 9053–9066, doi:10.1039/C9RA00490D.
75. Sotta, D. *MAT4BAT Advanced Materials for Batteries Project*; 2017; Available online: <https://cordis.europa.eu/project/rcn/109052/reporting/en> (accessed on 20 July 2019).
76. Schmalstieg, J.; Käbitz, S.; Ecker, M.; Sauer, D.U. A holistic aging model for Li(NiMnCo)O₂ based 18650 lithium-ion batteries. *Journal of Power Sources* **2014**, *257*, 325–334, doi:<https://doi.org/10.1016/j.jpowsour.2014.02.012>.
77. Nationalgrid ESO. *2019 four year ahead Capacity Auction (T-4) Delivery year 2023/24*; London, UK, 2020; Available online: <https://www.emrdeliverybody.com/CM/Auction-Results-1.aspx> (accessed on 06 May 2020).
78. National Grid. *Transitional Capacity Market Auction for 2016/17*; London, UK, 2016; Available online: <https://www.emrdeliverybody.com/CM/Auction-Results-1.aspx> (accessed on 30 April 2020).
79. National Grid. *T-1 Capacity Market Auction for 2018/19*; London, UK, 2018; Available online: <https://www.emrdeliverybody.com/CM/Auction-Results-1.aspx> (accessed on 30 April 2020).
80. Philippot, M.; Alvarez, G.; Ayerbe, E.; Van Mierlo, J.; Messagie, M. Eco-Efficiency of a Lithium-Ion Battery for Electric Vehicles: Influence of Manufacturing Country and Commodity Prices on GHG Emissions and Costs. *Batteries* **2019**, *5*, 23.
81. Li, J.; Cheng, Y.; Ai, L.; Jia, M.; Du, S.; Yin, B.; Woo, S.; Zhang, H. 3D simulation on the internal distributed properties of lithium-ion battery with planar tabbed configuration. *Journal of Power Sources* **2015**, *293*, 993–1005, doi:<https://doi.org/10.1016/j.jpowsour.2015.06.034>.
82. Tanim, T.R.; Rahn, C.D.; Wang, C.-Y. A Temperature Dependent, Single Particle, Lithium Ion Cell Model Including Electrolyte Diffusion. *Journal of Dynamic Systems, Measurement, and Control* **2014**, *137*, doi:10.1115/1.4028154.



© 2020 by the authors. Submitted for possible open access publication under the terms and conditions of the Creative Commons Attribution (CC BY) license (<http://creativecommons.org/licenses/by/4.0/>).